

See discussions, stats, and author profiles for this publication at: <https://www.researchgate.net/publication/354824635>

Impact of Carbon Fiber Reinforcement on Mechanical and Tribological Behavior of 3D-Printed Polyethylene Terephthalate Glycol Polymer Composites—An Experimental Investigation

Article in Journal of Materials Engineering and Performance · September 2021

DOI: 10.1007/s11665-021-06262-6

CITATIONS
31

READS
1,068



Impact of Carbon Fiber Reinforcement on Mechanical and Tribological Behavior of 3D-Printed Polyethylene Terephthalate Glycol Polymer Composites—An Experimental Investigation

Aysha Farzana Kichloo, Ankush Raina, Mir Irfan Ul Haq , and Mohd Shaharyar Wani

Submitted: 27 May 2021 / Revised: 17 August 2021 / Accepted: 3 September 2021

In this work, PETG-based composite polymer using fused deposition modeling technique has been developed with carbon fiber (CF) as the reinforcement. The effect of the carbon fiber and the process parameters (layer thickness, infill pattern, infill percentage) on the tensile, flexural strength, and the tribological behavior of the developed composite polymer has been investigated. The study revealed that addition of carbon Fiber 20 wt.% as a reinforcement in PETG resulted in a composite which exhibited better tensile strength with maximum improvement of 114% for triangular pattern and minimum of 43.7% for full honeycomb pattern. The bending strength also enhanced in case of CFPETG with a maximum of 25% increase in flexural strength for full honeycomb. The tribological testing revealed substantial decrease in the COF with the addition of carbon fiber. A reduction of around 47.3% at low speeds (100 RPM) and around 44.79% reduction at high speeds (500 RPM) in COF was achieved in comparison to PETG. The fractographic analysis and worn surface analysis revealed distinct fracture modes and wear mechanisms for different composite samples suggesting the role of CF in improving the properties of the developed composites. The study revealed that the developed 3D printed composite could help to widen the scope of PETG as an engineering material.

Keywords 3D printing, carbon fiber, flexural strength, fused deposition modeling, PETG, tensile strength, tribology

Abbreviations

3D	Three Dimensional
ABS	Acrylonitrile Butadiene Styrene
Al ₂ O ₃	Aluminum Oxide
CaCO ₃	Calcium Carbonate
CAD	Computer-Aided Designing
CF	Carbon Fiber
CFPETG	Carbon Fiber Polyethylene Terephthalate Glycol
CFPEKK	Carbon Fiber Poly Ether Ketone
CNT	Carbon Nano Tube
COF	Coefficient of Friction
FDM	Fused Deposition Modeling
GR	Graphite flakes
MWCNT	Multi-Walled Carbon Nano Tube
NASA	National Aeronautics and Space Administration
PC-ABS	Polycarbonate Acrylonitrile Butadiene Styrene
PEEK	Polyether Ether Ketone
PETG	Polyethylene Terephthalate Glycol
PLA	Poly Lactic Acid
SiO ₂	Silica
SL	Stereolithography
TGA	Thermogravimetric analysis
TiO ₂	Titanium Oxide
USA	United States of America
UV	Ultraviolet

1. Introduction

Owing to its technical, economic, and environmental benefits, 3D printing has emerged as a novel technology for rapid tooling and manufacturing of components with complex geometries and various other applications (Ref 1, 2). Presently, industries are facing a lot of challenges such as, the growing demand for tailored products, complexity in the equipment or products functions and structures, intense market competition, frequent design changes in the products (Ref 3, 4). Hence, there is a need to establish novel manufacturing techniques to shorten the production time and decrease the cost of production.

In a typical additive manufacturing process, a product is developed by providing an unique set of digital data (CAD data) to the machine that reduces the manufacturing cycle time (Ref 5) and results in low buy to fly ratio (ratio of weights of raw material and finished product), which ultimately reduces

Aysha Farzana Kichloo, Ankush Raina, and Mir Irfan Ul Haq, School of Mechanical Engineering, Shri Mata Vaishno Devi University, Jammu and Kashmir, Katra 182320, India; and **Mohd Shaharyar Wani**, Department of Metallurgical Engineering and Materials Science, IIT Bombay, Mumbai, India. Contact e-mail: haqmechanical@gmail.com.

the cost of final product. With almost 90% reduction in material wastage in comparison to conventional manufacturing processes (Ref 6), AMT can efficiently create high strength light

weight components by the use of technologies like CAE (Computer-aided engineering) and methods like finite element analysis (Ref 7, 8). Biomedical surgeries viz—Facial (Ref 9, 10), Neuro (Ref 11), Spine (Ref 12), Cardiovascular (Ref 13), Visceral (Ref 14) and several other implants (Ref 15) and prosthetics (Ref 16) are being successfully accomplished by AMT. Turbo-machinery (Ref 17, 18), and Automotive-related industries (Ref 19, 20) have also extensively employed this technology to develop intricate designs.

Thermoplastic polymer is being widely used for printing however due to its limited functionalities and mechanical properties, there is a dire need to design and develop novel materials which provide high performance and are sustainable (Ref 21, 22). Tailoring the desirable properties to explore the possibilities to develop various composites with unique properties is an emerging research area.

As per ASTM standards (Ref 23) FDM (fused deposition modeling) or also referred as FFF (fused filament modeling) is one of the most extensively used process owing to its various advantages (Ref 22, 24, 25). In FDM, the components are made up of strands or layers of molten polymer that flows out from a heated extruder. The quality and properties of the product depends upon various parameters which includes layer thickness, angle at which the layers are laid, speed of printing and distance between the layers (Ref 25–27). Despite the benefits like high-flexibility, low cost and simplicity of FDM process, there are some limitations like poor mechanical and surface qualities of the manufactured parts. The distortion between the internal layers (Ref 28) is the main limitation of this process.

Therefore, there is a need for the development of advanced and robust polymeric materials to widen the scope of this technology (Ref 29, 30). The common matrix material for AMT are thermoplastics, into which the filler components (fiber or particle-based materials) are added for the formulation of new material with better properties. Commonly used filler materials are carbon fiber (Ref 28), glass fiber (Ref 31), carbon nano tubes (Ref 32) which have resulted in the increased strength of the parent material. The exclusively used parent materials include poly lactic acid (PLA), acrylonitrile butadiene styrene (ABS), polyether ether ketone (PEEK), and polyethylene tetra glycol (PETG). However, carbon-fiber-reinforced thermoplastics are being widely preferred composite materials because of their recyclability and ease of manufacturing.

The carbon fiber in the form of powder was used as a reinforcement in PLA by Gavali et al. (2018). An increase in the tensile strength at 0, 90 raster angle in comparison to the raster angle of (45,45) corresponding to the layer thickness of 0.15 mm (Ref 33) has been observed. On adding carbon fiber (60 μm in length) to PLA in 5 wt.% and 7.5 wt.%, Ferreira et al. witnessed an increase of 22.5% in tensile strength, 21.86% in flexural toughness, 11.82% in flexural stress and 16.82% in flexural modulus with 5 wt.% carbon fiber. Also, on increasing the fiber content ductility, yield strength and toughness started to decrease and porosity became intense at 10% wt. fraction of carbon fiber (Ref 34). Addition of graphene platelets 10% by wt. into PLA, Prashantha et al. (2017) (Ref 35) found that the samples printed in the horizontal direction exhibited higher tensile strength (27%) and elastic modulus (30%) with decrease in break-strain values (due to poor adhesion and porosity). Coppola et al. (2018) (Ref 36) printed nano clay with PLA by melt extrusion and found an increase in elastic modulus and the storage modulus above glass transition temperature and 35°C was also found to be improve in the reinforced composite samples. Nakagawa et al. (2017)

reinforced ABS with carbon fibers of length 100 μm in percentages 5, 10, 15 by weight using double extrusion method (first extruded filament was microwaved) and found that the 3D-printed samples exhibited an increase in tensile strength along with better thermal stability (Ref 37). Yang et al. (2017) used continuous carbon fiber as filler material and followed direct addition method over the FDM machine and printed the samples which on testing revealed better flexural and tensile strengths, with flexural strength of 127 and 147 MPa tensile strength at 10% CCF. However, the performance at the interface was found to be display poor shear strength at inter-laminar zone (Ref 38). In a related study Dul et al. (2018) used the twin screw extruder method to make the reinforced ABS filaments with 1, 2, 4, 6 and 8% by weight of carbon nanotubes and printed samples by FDM. A decrease in the creep compliance, thermal expansion coefficient, and elongation at break were noticed and an increase in the tensile strength and moduli (but not vertical built) for 6% optimal wt. fraction was observed (Ref 32). A comparison between the properties of 3D-printed thermoplastic PETG and its carbon (20%) reinforced composite samples was carried out by Ferreira et al. (2018), wherein they found the Young's modulus, flexural strength and modulus of CFPETG improved by 70.10, 5.14, and 191.38%, respectively, compared to the PETG without any delamination (Ref 39). In a study Berretta et al. (2017) printed samples of PEEK with 1 and 5% CNT filler, improvements in the mechanical properties were observed, especially with 5% concentration CNT-PEEK, which displayed a decrease in both the tensile and shear strength (Ref 40).

In a study by Singh et al. (2017), silicon carbide 10% by wt. and aluminum oxide were added as reinforcements into Nylon 6 (50%), and the samples were printed successfully with FDM. Tribological tests on a pin-on-disk machine and reinforced composites for these samples displayed enhanced wear resistance and frictional coefficient than ABS (Ref 41). The effect on tribological behavior of the 3D printed PC-ABS samples for different values of FDM parameters viz—number of contours, build orientation, layer thickness, raster angle, and the coefficient of friction of the samples was found directly proportional to the layer thickness, build orientation, raster angle, and air gap (Ref 42). Also, the rate of wear was found inversely proportional build orientation and layer thickness and directly proportional to air gap and raster angle (Ref 43). Nanoaluminum oxide (14%) was used as reinforcement to Nylon 6 (86%) for enhancing the wear behavior in grinding applications of rapid tooling in an investigation by Boparia et al. (2018). On testing the printed samples with pin-on-disk arrangement, the nanocomposite showed less material loss, wear, frictional force and coefficient of friction than ABS and hence, promising in grinding applications of rapid tooling (Ref 44). In a tribological study of 3D-printed PLA with added graphene, Bustillos et al. (Ref 45) reported that Graphene-PLA composites were more resistant to wear (14%) and also exhibited lower frictional coefficient. Similarly, Ertane et al. (Ref 46) developed biogenic carbon and used it as a reinforcement to PLA with three concentrations by wt. 5, 15, and 30%. Wear studies were made using the ball-on-disk arrangement (Aluminum Oxide ball) with dry sliding conditions, the 30% concentration biocarbon-PLA composite exhibited minimum wear with coefficient of friction being slightly affected by all the concentrations.

In a study by Kui Wang et al. where filament of PLA with carbon fiber reinforced was 3D printed and testings were performed to investigate the effects of infill pattern (triangular and hexagonal), infill percentage (29, 39, and 49%) and strain

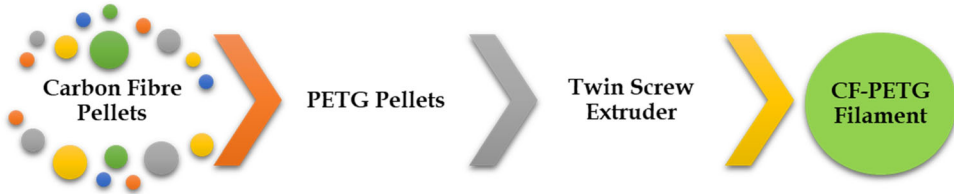


Fig. 1 Methodology for CF-PETG filamentation

rate on mechanical properties of the specimens. The hexagonal pattern offered higher tensile strength and modulus but elongation at break was lower than for triangular pattern, at certain infill percentage. The Young's modulus and strength increased with increase in infill percentage and the strain rates whereas the relative energy absorption increased with increase in strain rates for all infill patterns (Ref 47). Similarly, Kamaal et al. (2021) studied the effect of layer thickness(0.2, 0.25, and 0.3 mm), build orientation(x, y, z-axis) and infill percentage (20, 50, 80%) on the carbon fiber-reinforced PLA-printed samples keeping grid as the infill pattern for all samples. In tensile testing, strength was found to increase with layer thickness and percentage of infill whereas in Izod test build orientation and percentage of infill were found to greatly affect the strength than the layer height and hence some optimum conditions were concluded for both the tests as per 'Technique for Order Preferences by Similarity to Ideal Solution' (Ref 48). A carbon fiber-reinforced composite of polyether ketone ketone (PEKK) was 3D printed by Nachtane et al. (Ref 49) with infill percentage of 20, 50, and 100% and were compressed using Split Hopkinson Pressure Bar for impact pressures 1.4, 1.7, 2, and 2.7 bar. Also, the dynamic behavior was tested for repeated impact loading at 100% infill percentage. The results of this work presented that higher infill percentage went under less deformation and hence more strength. Also, the high density prints are beneficial for dynamic compression and low density prints are beneficial for cost and time optimization. Kumar et al. printed the PETG and CFPETG (CF-20%) samples with infill percentages 25, 50, 75, and 100%. After annealing these samples were tested and compared for tensile, flexural, impact strength, and hardness. The findings of this experimental work demonstrated that CFPETG samples presented better results for all tests in comparison with PETG, especially at 100% infill density where maximum improvement was seen (Ref 50).

In view of the above discussion, it can be concluded that despite PETG being a promising 3D printable material, a detailed study to elucidate the effect of various 3D printing process parameters on the tensile and flexural strength of PETG and CF reinforced PETG has not been attempted so far. Also, the tribological behavior of the PETG carbon fiber composite has not been explored in detail. Therefore, the current study was undertaken to address the aforementioned gap.

2. Materials and Methods

2.1 Sample Details

2.1.1 Materials. The polymer matrix used in this work is polyethylene terephthalate glycol (PETG) and carbon fiber reinforced PETG (CFPETG) (20 wt.%). The PETG filament with 1.75 ± 0.05 mm diameter and $1.27\text{g}/\text{cm}^3$ density was

procured from *Solidspace Filament Ltd.*. The CFPETG composite was prepared by melt extrusion method, PETG pellets and carbon fiber ($100 \mu\text{m}$) (Procured from Colorfabb) were converted into filament with $1.75\text{mm} (\pm 0.05)$ diameter, $1.370\text{g}/\text{cm}^3$ density by double extrusion (microwave oven was used after first extrusion) via screw extruder with constant rotational speed (60 RPM) and temperature 230°C , depicted in Figure 1.

2.1.2 Sample Preparation. The CAD models were made as per ASTM D638-(I) with dimensions $165 \times 19 \times 3.2$ mm for tensile testing and as per ASTM D790 with dimensions $80 \times 10 \times 4$ mm for flexural testing and a cylindrical block of dimensions $12 \times 12 \times 12$ mm for tribological testing software "Creo" as shown in Figure 2. The G-codes were generated by using slicing software "Simplify 3D." All the specimens were made as per ASTDM standards already mentioned above using FDM 3D Printer (Atharva Mega Make) (Figure 3), and the technical specifications are given in Table 1.

For this study, critical parameters such as layer thickness, raster angle, infill pattern, infill density were varied during printing process primarily on the basis of trial testing and as per previous studies; however, bed temperature, extruder temperature, print speed, orientation, multiplier were set constant (Ref 9, 51, 52). The details about the process parameters are enlisted in Table 2. To print PETG samples, a brass nozzle was used whereas for carbon fiber reinforced samples stainless steel nozzle was used. The prepared sample combinations are enlisted in Table 3. The tribological samples of both the materials PETG and CFPETG were printed as cylindrical pins as shown in Figure 3(c) of diameter 12 mm and height 12 mm with three different layer thickness (0.1, 0.14, 0.18mm).

2.2 Testing Methodology

2.2.1 Tensile and Flexural Testing. The tensile test samples were printed as per the ASTM-D638-(I) standard as shown in Figure 4(a) and (b), the tests were performed using Tensometer (PC 2000) with load cell of 2 kN speed 3mm/min. The bending test samples were printed as per the ASTM-D790 standard as shown in Figure 4(c) and (d), the three-point bending tests were performed using three-point bending using a Universal Testing Machine. The samples were subjected to loading till occurrence of fracture. SEM images of the fractured samples were captured post to testing and were analyzed to study the various modes of fracture. Each test was repeated thrice and a mean value is reported to ensure repeatability of data.

2.2.2 Tribological Testing. The samples for frictional testing were prepared as cylindrical pins with diameter 12mm and height 12mm as shown in Figure 4(e) and (f). The samples were made of both the materials PETG and CFPETG with three different layer thickness (0.1, 0.14, and 0.18). The tests were performed as per ASTM G99 standard under dry sliding

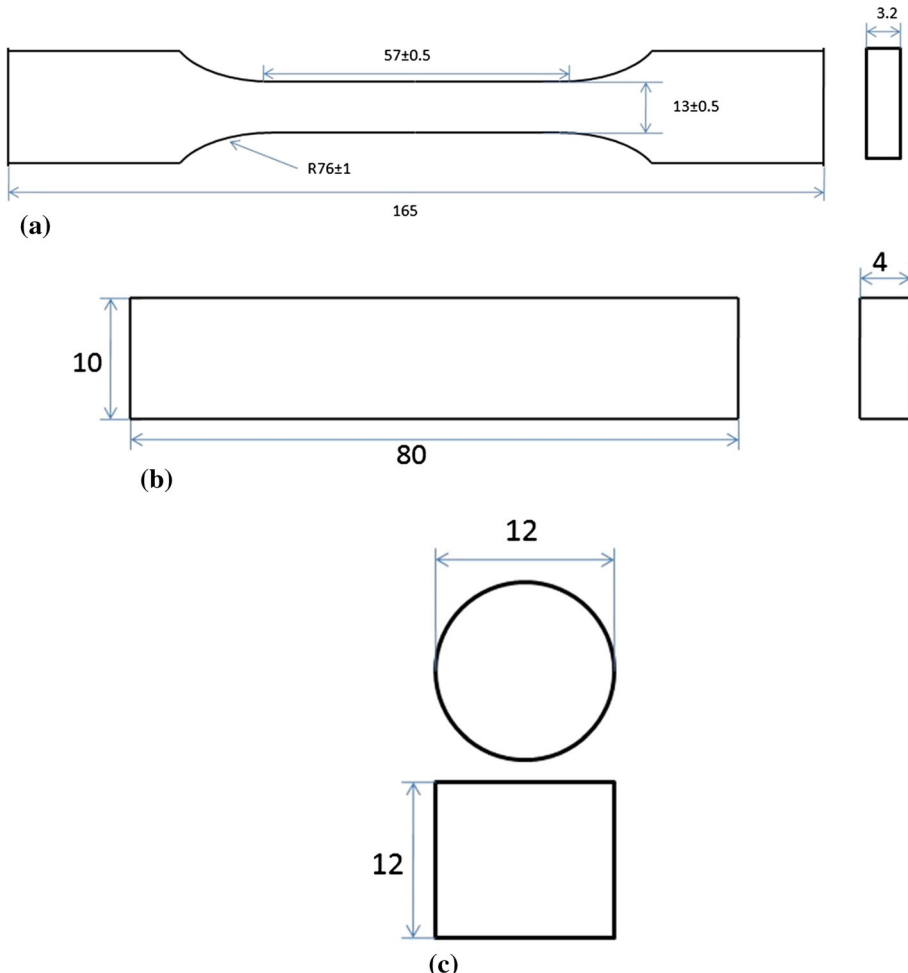


Fig. 2 Geometrical details of (a) Tensile sample as per ASTM D638 (b) Bending sample as per ASTM D790 (c) Tribological sample in millimeters

condition using a pin-on-disk tribometer (DUCOM India) with EN31 steel disk as a counterface (Figure 5). The tribometer used in is a computer integrated machine pin-on-disk Tribometer (DUCOM Made TR-20LE-PHM400) having a load cell to track the COF with a load range of up to 200 N, maximum RPM of around 2000RPM.

The samples were tested under five different loads (10, 20, 30, 40, and 50 N) at high speeds and low speeds (500 RPM/ 5.24m/s and 100 RPM/1.05m/s). The wear track diameter and sliding distance were kept constant as 100 mm and 1500 m, respectively. SEM analysis was carried out to study the morphologies obtained after different modes of testing. The tribological testing was repeated thrice, and a mean COF value is reported.

3. Results and Discussions

3.1 Tensile Strength

3.1.1 Effect of Infill Pattern on Tensile Strength. Figure 6 shows the variation of tensile strength corresponding to type of infill pattern for a constant layer thickness 0.1mm It can be observed that the honeycomb pattern showed better tensile

strength than the triangular pattern particularly at 70% with a max increase of 27% for PETG and 39% for CFPETG and at 100% infill percentage, with a max increase of 45% for PETG and 38% for CFPETG. The behavior of patterns from Figure 6 could be attributed to the fact that the grid and honeycomb infill patterns perform structurally better and lead to better distribution of stresses. However, for a layer thickness of 0.14 mm (Figure 7), it was observed that grid pattern exhibited good tensile strength compared to other two patterns with an increase of 25% for PETG and 8.9% for CFPETG in comparison to triangular pattern and an increase of 11.2% for PETG and 10% for CFPETG than honeycomb patterns at an infill of 70%. These results are found consistent with Menderes et al. (Ref 51). Also, for the layer thickness 0.18 mm (Figure 8) triangular pattern exhibited the maximum tensile strength followed by honeycomb and grid patterns. This may be due to the inability of the process to generate the proper infill for honeycomb at 0.18mm layer thickness as has also been reported in the literature (Ref 53).The behavior of the honeycomb pattern showing better results for 0.1mm thickness is attributed to the fact that at lesser layer thickness the geometry of the infill patterns is more effective than for higher thicknesses where geometry becomes less effective and hence toughness of the structures do not vary a lot.

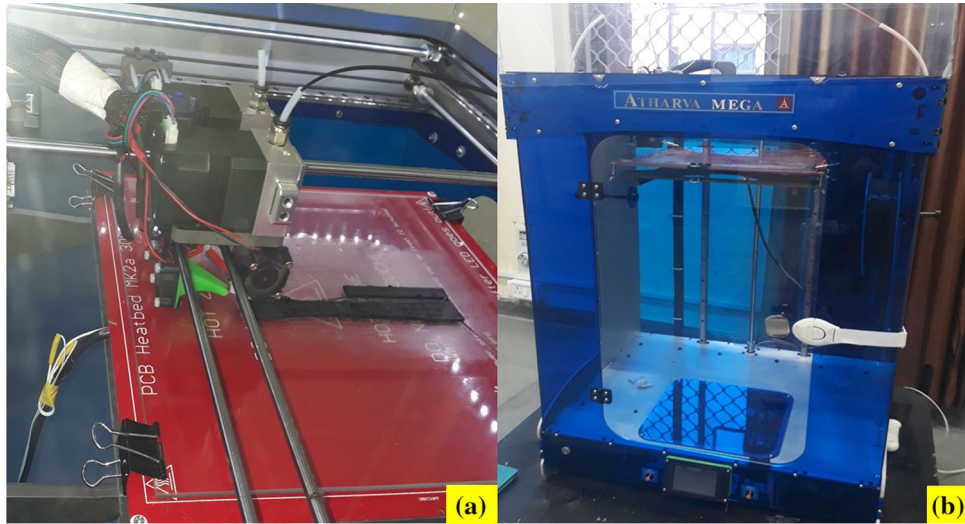


Fig. 3 FDM-based 3D printer (a) during printing (b) full machine

Table 1 Technical specifications of Atharva Mega 3D Printer

S.No.	Entity	Description
1.	Physical dimensions	620×520×965 mm
2.	Technology	Fused deposition modeling
3.	Extruders no.	2
4.	Layer resolution	0.04-0.2 mm (for 0.4mm nozzle dia)
5.	Nozzle diameter	1.75mm
6.	Filament material	PLA, ABS, Nylon, Ninja Flex, PETG, Wood, PLA/PHA,PETG,POM
7.	XYZ accuracy	12.5, 12.5,5 micron
8.	Print head	Swappable nozzles (0.2,0.3,0.4,0.5,0.6mm)
9.	Supported OS	Windows
10.	Power Supply	Input 120/240V AC, Output 24V DC 20A
11.	Operating ambient temp.	15-35 degree
12.	Build Volume	290 × 290 × 500 mm
13.	Nozzle Temperature	300 °C
14.	Print Speed, , 3.5 inch color	20-300mm/s
15	Build plate temperature	50° to 100 °C

Table 2 Process parameters chosen for printing samples

S.No.	Parameters	Values
1.	Nozzle dia	1.75mm
2.	Nozzle material	Brass, stainless steel
3.	Bed temp	75°C
4.	Extruder temp	262°C (CFPETG),235°C (PETG)
5.	Print orientation	Flat
6.	Print speed	50mm/s
7.	Multiplier	1.1(CFPETG),0.95(PETG)
8.	Raster angle	[45, -45]
8.	Layer thickness	0.1, 0.14, 0.18
9.	Infill pattern	Grid, Full honeycomb, Triangle
10.	Infill density	40, 70, 100%

3.1.2 Effect of Infill Percentage on Tensile Strength. Figure 6–8 bring into picture the effect of the infill percentage on tensile strength wherein it can be observed that tensile strength is enhanced with the increase in infill percent-

age with most of the layer thicknesses and patterns. Out of all the three layer thicknesses, at layer thickness 0.14mm, a max increase of 87% (PETG- triangular pattern) and 39% (CFPETG- honeycomb) in tensile strength was observed from 40% infill to 100% infill percentage. This general trend of increase in tensile strength with the increase in infill percentage can be attributed to the decrease in air gap and increase in density. The reduced air gap and the increased density reduces the chances of deformation. The improvement in the bonding strength between the subsequent layers due to reduction in air gaps also contributes to this behavior. But for layer thickness 0.18mm, the grid and triangular patterns have shown a decrease in strength in case of PETG. Moreover, the results of triangular pattern in case of CFPETG are not in accordance with the results of other layer thicknesses. These results can be attributed to the domination of imperfections at the joining nodes generated by the process at high layer thickness and infill percentage (100%). Similar trends in tensile strength have been previously studies (Ref 54–57).

Table 3 Details of sample combination

Sample No.	Layer thickness	Infill pattern	Infill percentage
1.	0.1	Grid	40
2.		Grid	70
3.		Grid	100
4.		Full honeycomb	40
5.		Full honeycomb	70
6.		Full honeycomb	100
7.		Triangle	40
8.		Triangle	70
9.		Triangle	100
10.	0.14	Grid	40
11.		Grid	70
12.		Grid	100
13.		Full honeycomb	40
14.		Full honeycomb	70
15.		Full honeycomb	100
16.		Triangle	40
17.		Triangle	70
18.		Triangle	100
19.	0.18	Grid	40
20.		Grid	70
21.		Grid	100
22.		Full honeycomb	40
23.		Full honeycomb	70
24.		Full honeycomb	100
25.		Triangle	40
26.		Triangle	70
27.		Triangle	100

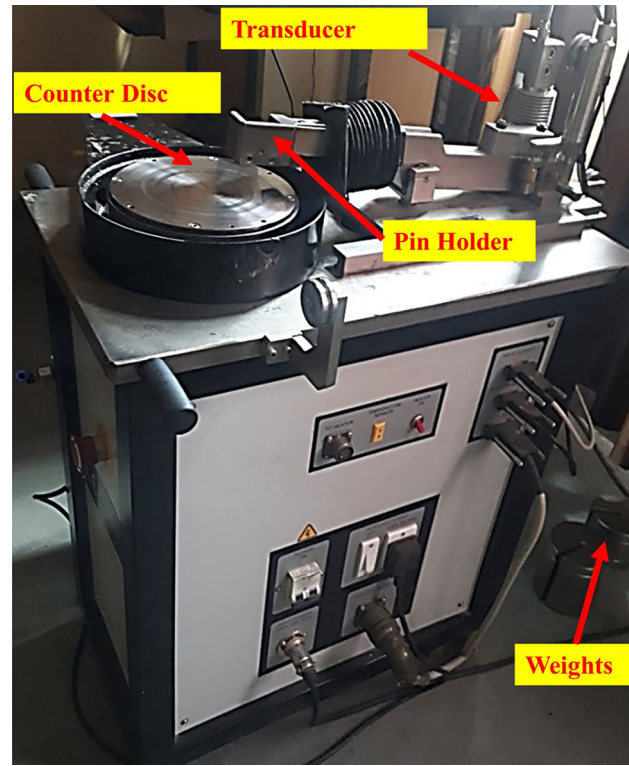


Fig. 5 Representative image of pin-on-disk tribometer

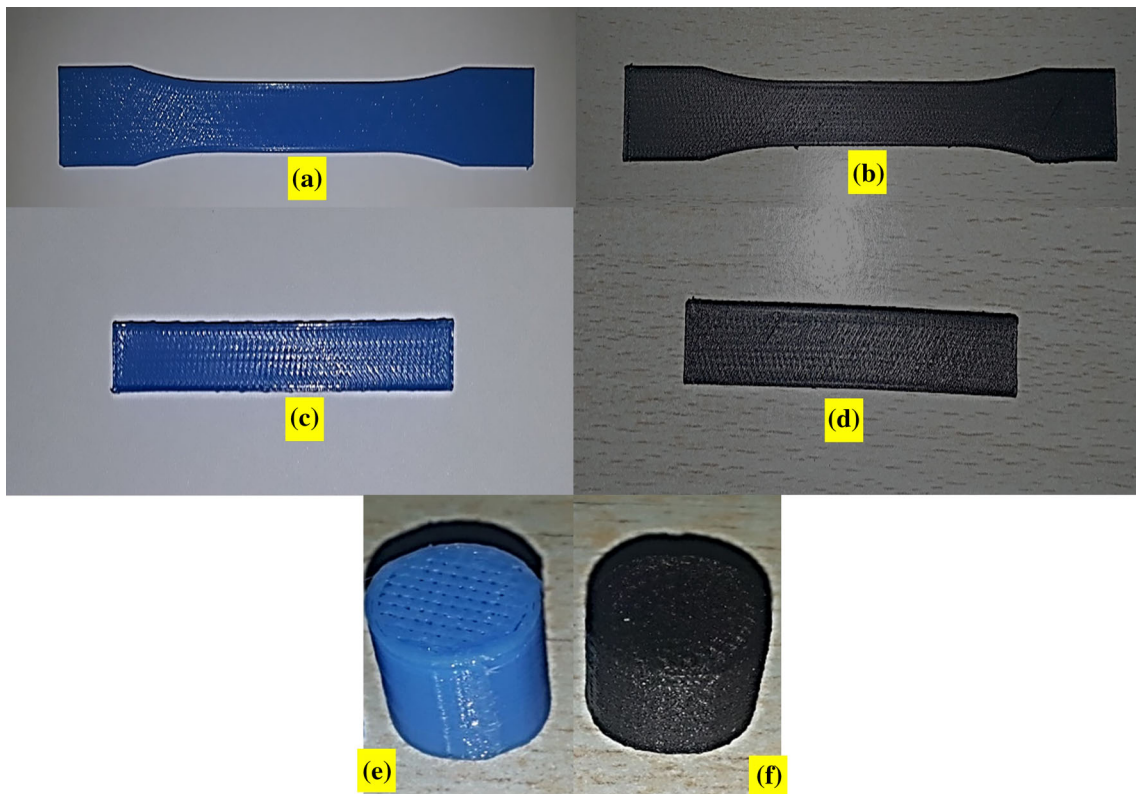


Fig. 4 Representative images of tensile test samples (a) PETG (b) CFPETG, bending test Samples of (c) PETG (d) CFPETG and tribological samples of (e) PETG and (f) CFPETG

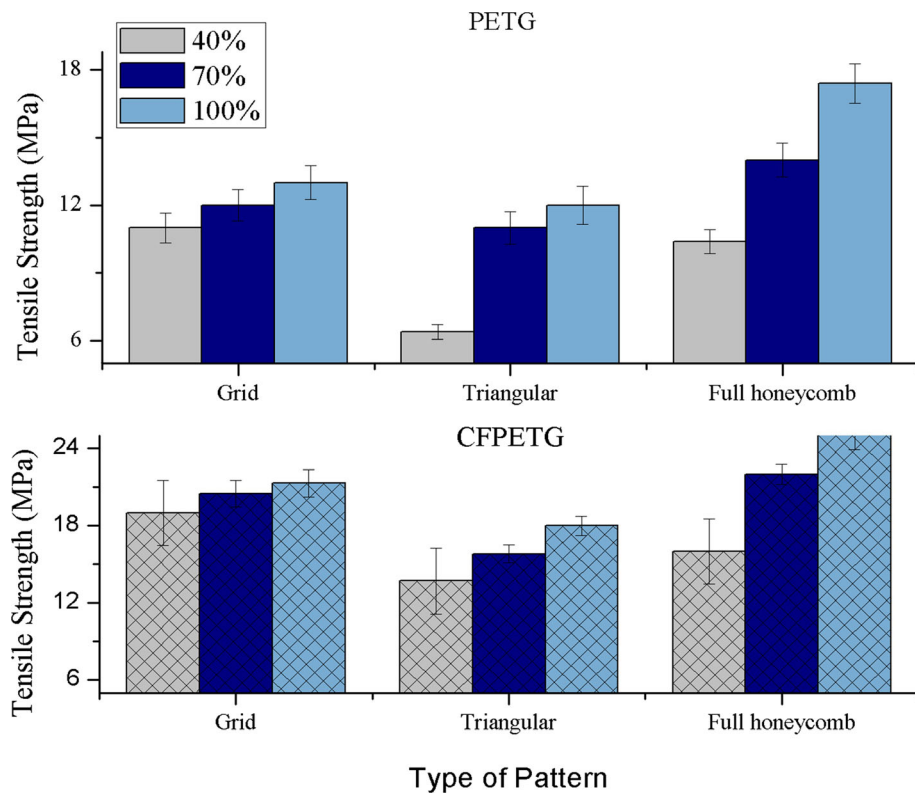


Fig. 6 Variation in tensile strength with infill pattern and percentage with constant layer thickness (0.1mm)

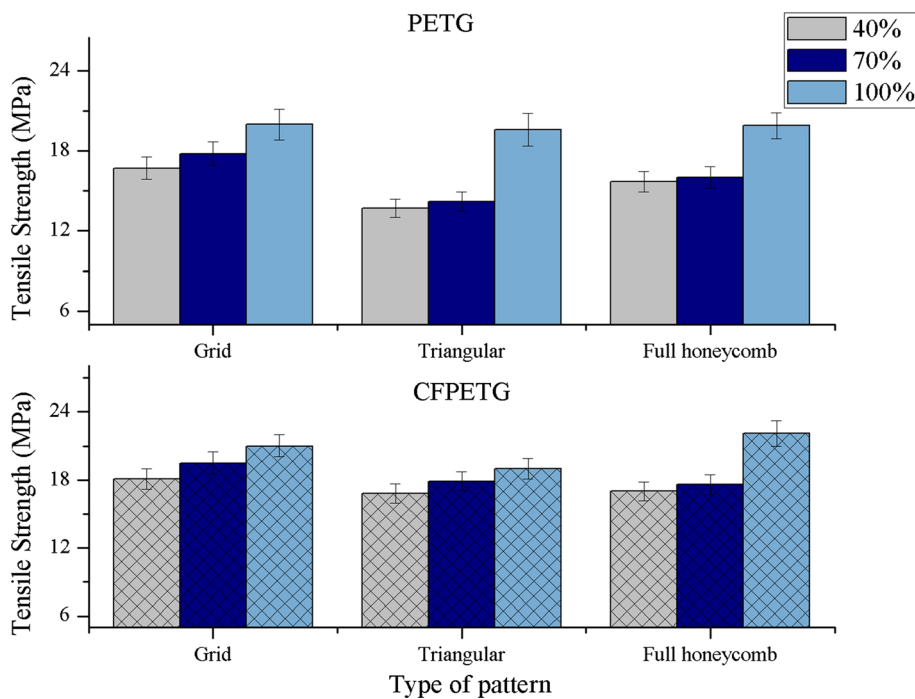


Fig. 7 Variation in tensile strength with infill pattern and percentage with constant layer thickness (0.14mm)

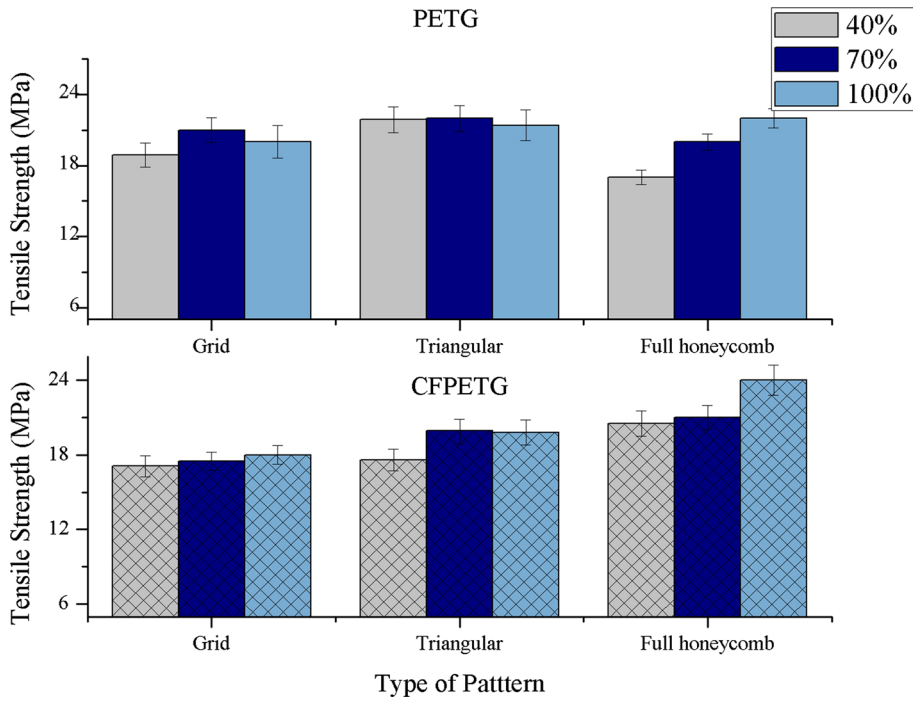


Fig. 8 Variation in tensile strength with infill pattern and percentage with constant layer thickness (0.18mm)

3.1.3 Effect of Layer Thickness on Tensile Strength.

From Figure 6–8, it can be seen that with the increase in layer thickness the tensile strength exhibited increasing trend for triangle and honeycomb patterns. From layer thickness 0.1mm to 0.18mm, a max of 242% (PETG-triangular pattern) and 28% (CFPETG-honeycomb pattern) increase in strength was observed at 40% infill percentage. This increase can be justified by the fact that on increasing the layer thickness the number of layers in the specimen decreases which means that there will be fewer bonding zones during the tensile testing. The decrease in the void formation in case of increased layer thickness due to a smaller number of bonding zones also improves the strength.

Whereas for grid pattern strength was found to remain least affected on going from layer thickness 0.1mm to 0.14mm but a decrease in strength was observed for 0.18mm layer thickness in case of CFPETG. In the grid pattern, the bonding zone between the layers corresponds only with the points where the filament crosses the previous layer filaments. Also, grid has least strength to weight ratio out of the three patterns possibly resulting in the said behavior. But in case of PETG grid pattern showed increase in strength with layer thickness 0.14mm and then at 0.18mm layer thickness strength was found to decrease slightly at 100% than at 70% infill percentage. The reason here can be the poorly generated structures at higher layer thickness. The kind of behavior was also reported in the previous studies (Ref 51, 58).

3.1.4 Effect of Carbon fiber Reinforcement on Tensile Strength.

Figure 7 shows the effect of addition of carbon fiber as reinforcement to PETG on tensile strength, an improvement in the tensile strength for most of the patterns and percentages has been observed. At layer thickness of 0.1 mm, the strong adhesion between the layers at the interface may have contributed to the enhanced tensile strength. Carbon fiber have been extensively used to enhance the strength of printed specimens owing to their high strength to weight ratio (Ref 59,

60).

From Figure 7 for layer thickness revealed that the addition of carbon fiber in the polymer have not produced a considerable improvement. It may be due to poor interfacial interactions at higher layer thickness due to little or no chemical bonding. Moreover, the carbon fibers are separated from the sample during the tensile test as reported in the literature (Ref 61).

Figure 8 showing behavior of tensile strength with different infill patterns at a constant layer thickness of 0.18mm reveals that there is very less or no improvement in tensile strength with the addition of carbon fiber. The grid and triangular patterns have shown a decrease in strength on addition of carbon fiber reinforcement. A significant improvement in strength has been observed for full honeycomb pattern. In the full honeycomb pattern, each layer lays down on a similar previous layer. However, in the grid and triangle pattern, the bonding zone between the layers corresponds only with the points where the filament crosses the previous layer filaments which contributed to an insignificant enhancement in strength. Also, the difference in stress and weight distribution of the patterns can lead to this result which is in line with the study (Ref 53).

In view of above discussion, it can be envisaged that at the layer thickness 0.1mm and 0.14mm with different infill pattern and percentage the tensile strength increased with the increase in layer thickness in case of PETG. The CFPETG showed better tensile strength in comparison to PETG at lower layer thickness however for higher layer thickness CFPETG strength is not providing good results. Among three pattern grid and honeycomb showed good strength with maximum strength at 100% infill for both PETG and CFPETG. But, the maximum percentage improvement in strength in case of all the layer thicknesses with addition of carbon fiber was observed with triangular pattern. Adding carbon fiber to PETG improved tensile strength upto 114% at 0.1mm layer thickness with 40% infill percentage, 26% at 0.14mm thickness with 70% infill

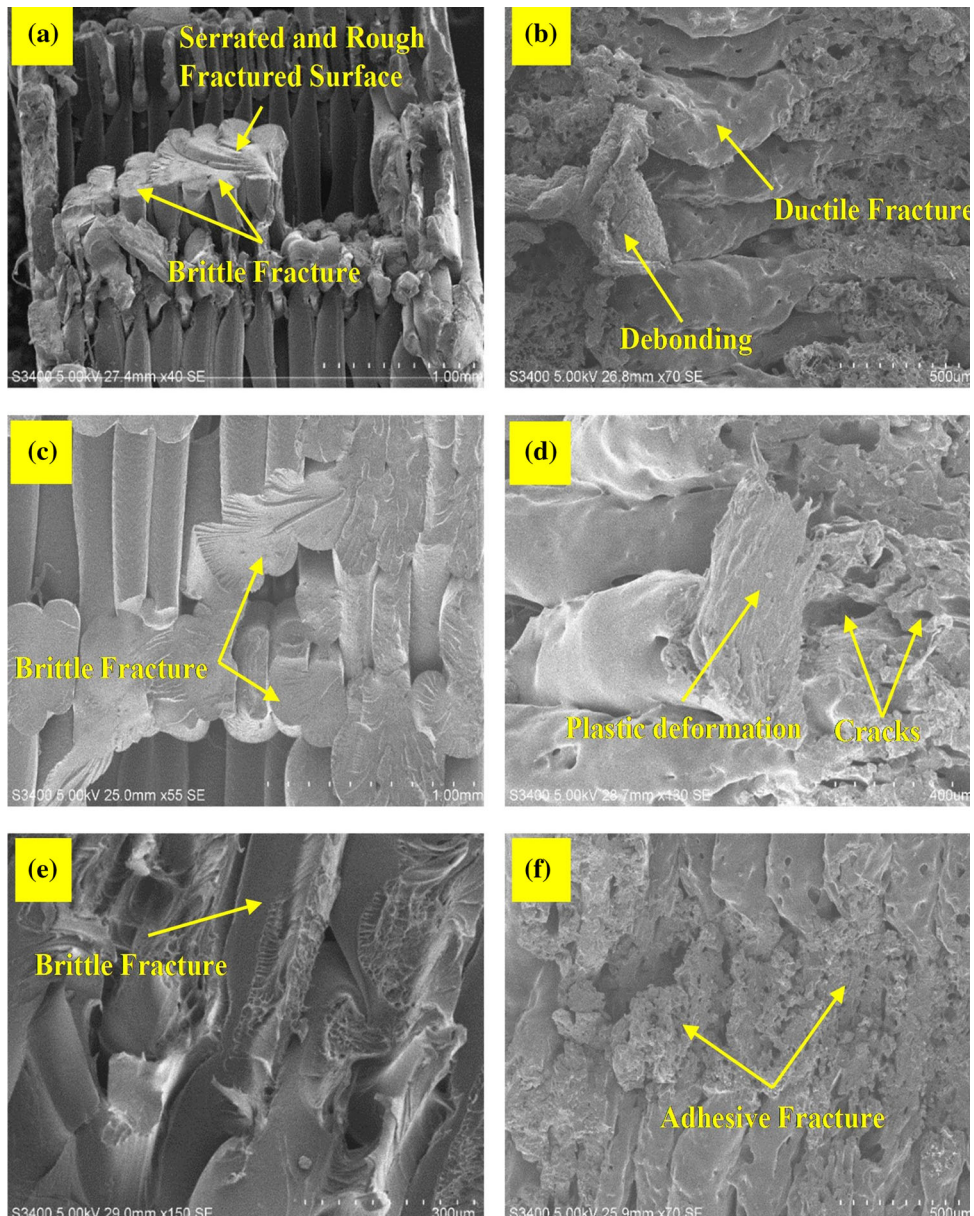


Fig. 9 SEM fractographic images of tensile tested samples (a) grid pattern PETG (b) grid pattern CFPETG (c) triangular pattern PETG (d) triangular pattern CFPETG (e) honeycomb PETG (f) honeycomb CFPETG corresponding to infill percentage of 70% and layer thickness of 0.14mm

percentage and at 0.18mm an increase of 24% with 40% infill percentage for triangular pattern.

3.1.5 SEM Fractography of Tensile Samples. Figure 9 shows the fractographic images of the tensile samples after the testing. An inter-layer and intra-layer fracture is visible from the SEM images. Also, different bonding zones between the subsequent layers can be observed for the three types of infill patterns. This plays a significant role in the stress distribution and the mode of fracture. It is evident from the fractographic images that in case of PETG samples the fracture type is brittle fracture in comparison with the CF-PETG samples, wherein the

fracture is adhesive. Some serrated and rough fractured surfaces are also visible in Figure 9. Some interesting features which can be observed include debonding, plastic deformation, cracks, necking.

3.2 Flexural Strength

3.2.1 Effect of Infill Pattern on Flexural Strength. It can be seen from Figure 10 and 11 that at a layer thickness of 0.1 mm as well as 0.14 mm, the grid and triangular patterns exhibited good flexural strength out of all the three patterns for both PETG as well as CF-PETG samples. The percentage

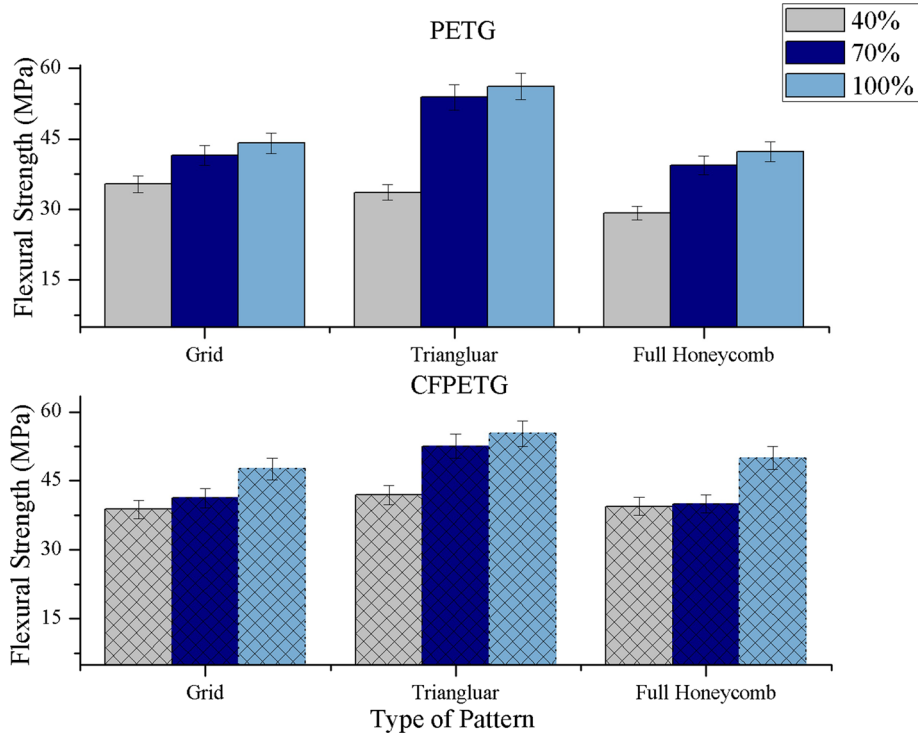


Fig. 10 Variation in flexural strength with infill pattern and percentage with constant layer thickness (0.1 mm)

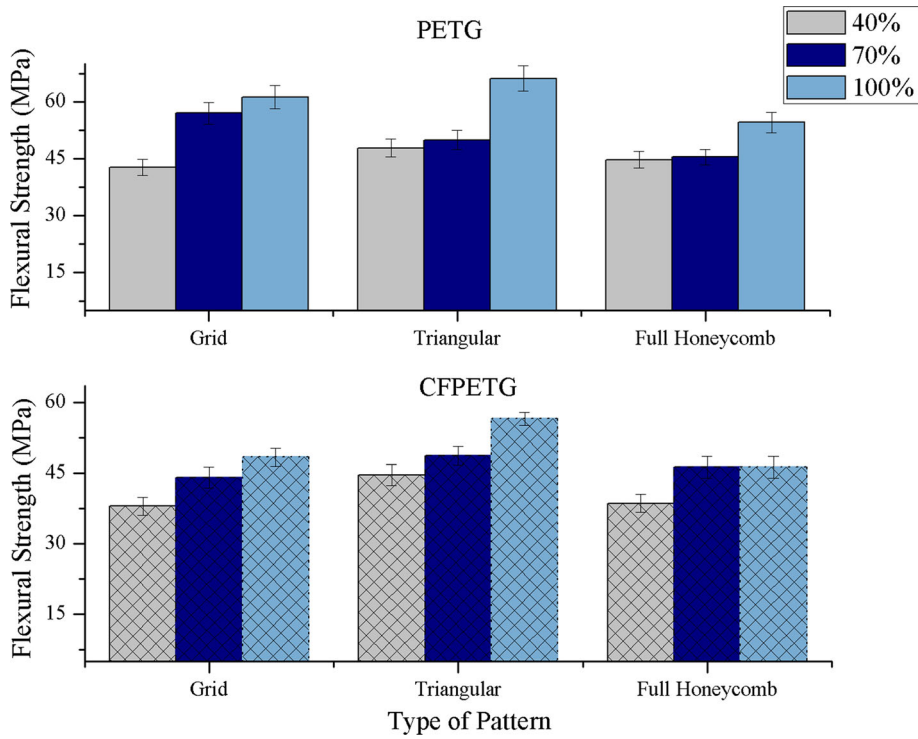


Fig. 11 Variation in flexural strength with infill pattern and percentage with constant layer thickness (0.14mm)

improvement in case of triangular pattern compared to honeycomb at 0.14mm thickness was 21% for PETG and 22% for CF PETG at 100% infill. In case of the 0.18 mm layer

thickness also a similar behavior was observed for PETG samples, however the full honeycomb pattern exhibited better flexural strength for CF PETG samples (Figure 12). The good

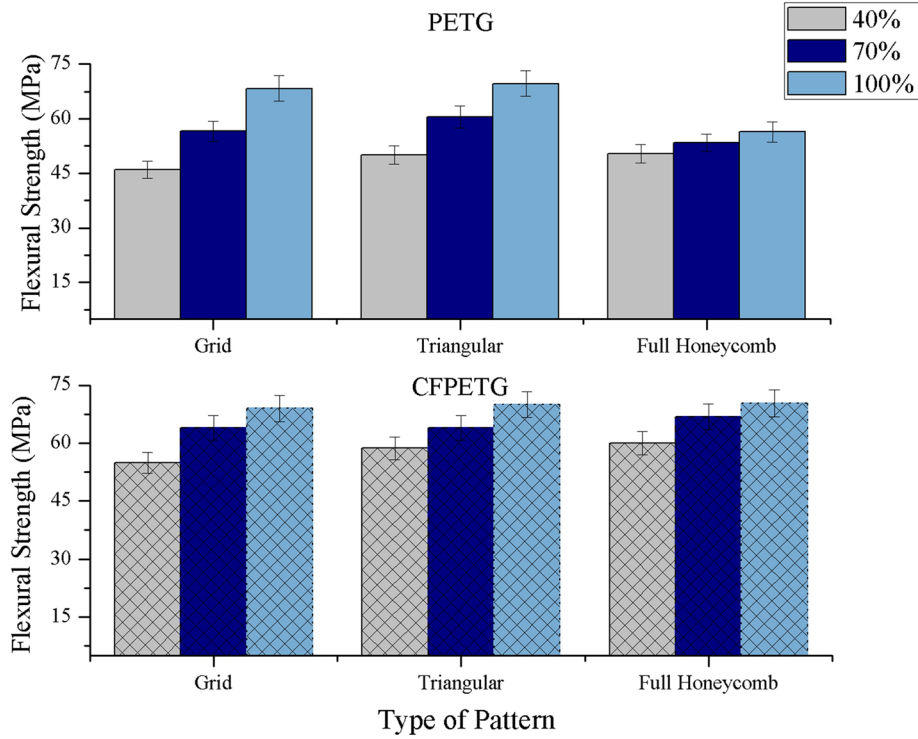


Fig. 12 Variation in flexural strength with infill pattern and percentage with constant layer thickness (0.18mm)

flexural strength exhibited by grid and triangular patterns can be attributed to the less residual stress accumulations in case of grid and triangle as bonding zone is formed only at the points where filament crosses the previous layer filament unlike in honeycomb where each layer lays down on previous layer (Ref 51, 51, 62). The observed behavior is also due to the intrinsic nature of the infill patterns to deform and absorb the stress before the bonds between the different fibers break.

3.2.2 Effect of Infill Percentage on Flexural Strength.

As evident from Figure 10–12 corresponding to layer thickness of 0.1mm, 0.14mm, and 0.18mm respectively, a trend similar to tensile testing, i.e., strength increases with the increase in infill percentage at all the infill patterns can be observed. Flexural strength increased upto 43% for PETG and 27% for CFPETG from 40 to 100% infill percentage for grid pattern at layer thickness of 0.14mm. This improvement with the increase in infill percentage can be attributed to the reduction of air gap between the layers as the thickness of layers increases leading to the increase in the flexural strength. The decrease in the porosity and void content also contributes to this behavior as the voids act as potential sites of crack nucleation. This result was found in accordance with the previous studies (Ref 63).

3.2.3 Effect of Layer Thickness on Flexural Strength.

Layer thickness has a positive impact on the flexural strength (Figure 10–12). From 0.1mm layer thickness to 0.18mm layer thickness, an improvement of 33% for PETG and 40.6% for CFPETG at 100% infill percentage for honeycomb pattern was observed. This behavior can be attributed to the decrease in number of layers and number of bonding zones. According to the earlier findings, it has been suggested that parts should be generally built with minimum number of layers in order to minimize the distortions due to stress accumulation (Ref 64). The weak bonding between the subsequent layers reduces the strength of a 3D printed part. Consequently, 3D printing with

minimum layers contributes toward improvement in strength. However, to capture the geometry of a part, the number of layers can't be decreased beyond certain limit.

3.2.4 Effect of Carbon fiber Reinforcement on Flexural Strength.

As evident from Figure 10 and 11, the addition of carbon filler did not alter the flexural strength by a considerable amount at lower layer heights particularly at 0.14mm where a decrease in flexural strength can be observed. This can be attributed to the weak interlayer and matrix to filler bonding probably occurred due to residual stresses caused by volumetric shrinkage of the polymer layers during solidification from the melt. Weak interlayer bonding may also be caused by the low molecular diffusion and low cross-linking between the polymer layers during deposition from the melt. In addition, the interlayer porosity reduced the load-bearing area across the layers and hence provided an easy fracture path (Ref 62, 65). The addition of carbon fiber increases the matrix-filler interface in addition to the interface at the inter-layers. So, there are two factors which contribute toward the strength (a) intrinsic characteristics of the filler which may improve the strength (b) increased matrix-filler interface area leading to increase in the void content.

Figure 12 shows the effect of addition of reinforcement of carbon fiber on the flexural strength of polymer wherein it can be seen that there is an improvement in the flexural strength for all the infill patterns and infill percentages. The maximum improvement with addition of carbon fiber was upto 25% for full honeycomb pattern at layer thickness 0.18mm with 70% infill percentage. The effect of increase in flexural strength with the increase in layer thickness proved well with the case of reinforcement (Ref 64). The better aspect ratio of the carbon fiber filler increased the flexural strength of the composite as it was reported by Wypych (2016) that the flexural strength depends upon the aspect ratio of the particle (Ref 66). Several

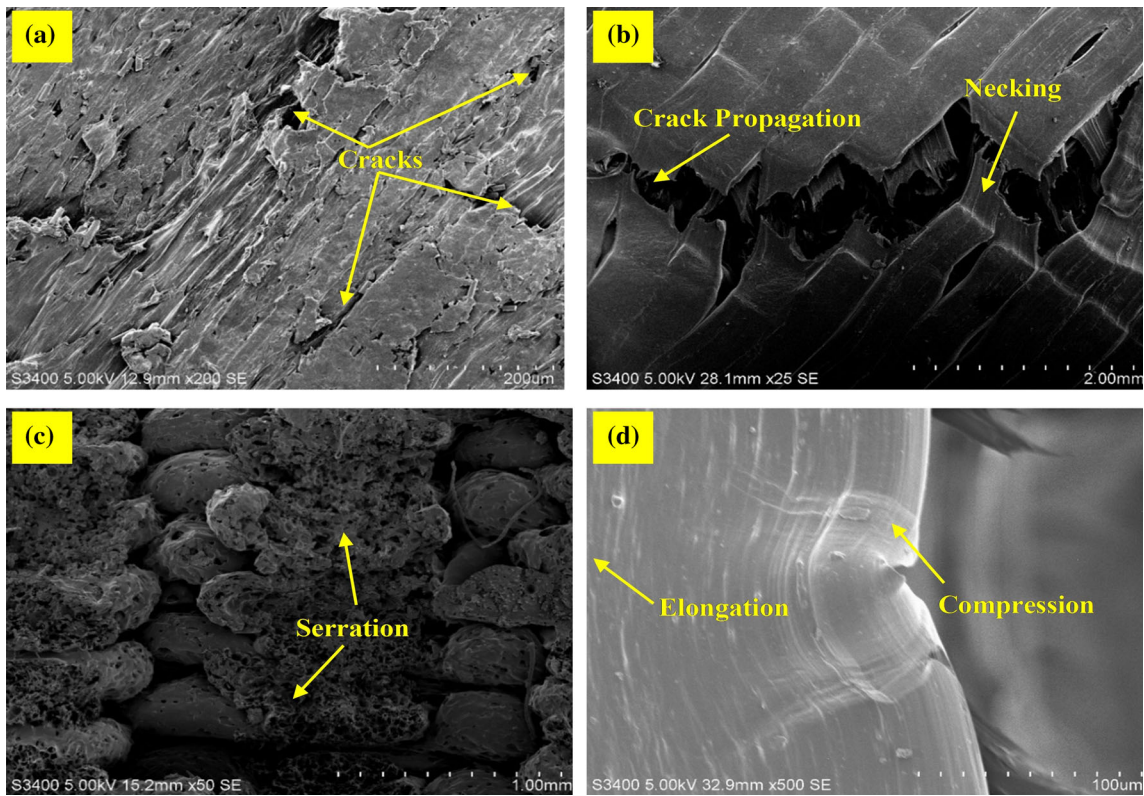


Fig. 13 SEM fractographic images of flexural tested samples (a) grid PETG (b) grid CFPETG (c) honeycomb PETG (d) honeycomb CFPETG corresponding to infill percentage of 70% and layer thickness of 0.14mm

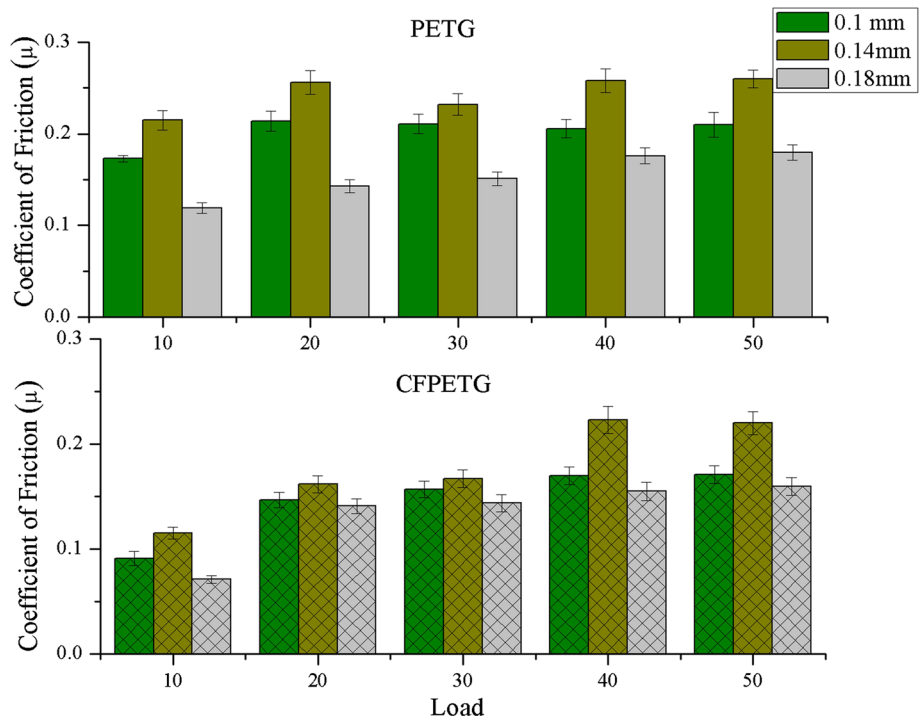


Fig. 14 Variation of coefficient of friction with load at 100 rpm

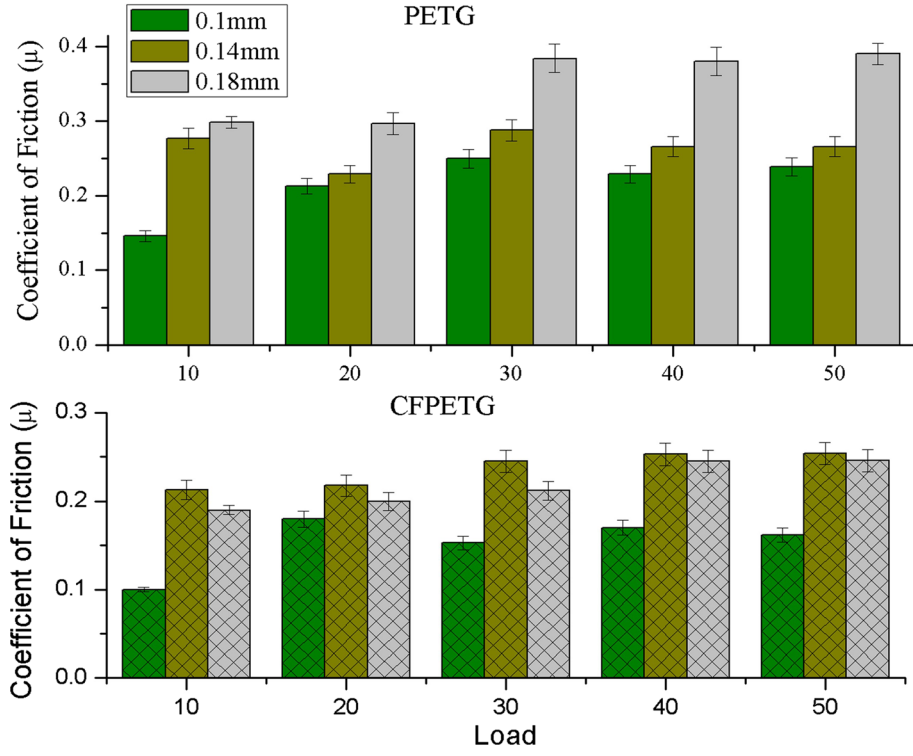


Fig. 15 Variation of coefficient of friction with load at 500 rpm

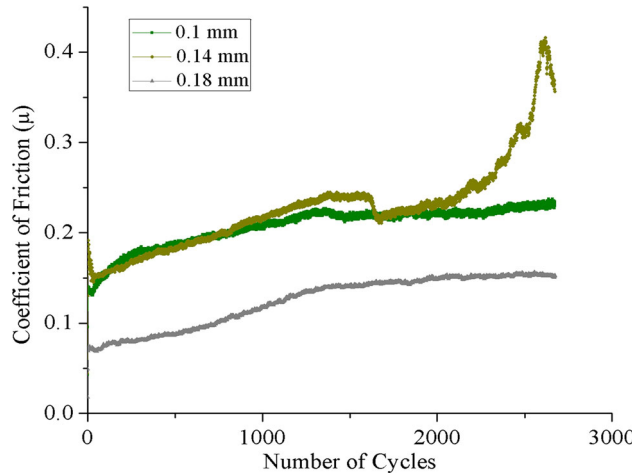


Fig. 16 Variation in COF with number of cycles at 30N and 100 rpm for PETG

other studies have also revealed that high flexural strength is attained at higher layer thicknesses (Ref 37, 39).

3.2.5 SEM Fractography of Flexural Samples. Figure 13 shows the representative SEM fractographic images of the samples after the flexural testing. Some cracks are visible on the fractured surface (Figure 13a). In Figure 13(b) the crack formation and the mode of fracture can be seen, wherein it is evident that the crack follows the path of the bonding zones which is a weak region. Some elongation/necking prior to the fracture is also visible in Figure 13(b). Some fibers being pulled out can also be seen in Figure 13(c). Also, a serrated fractured

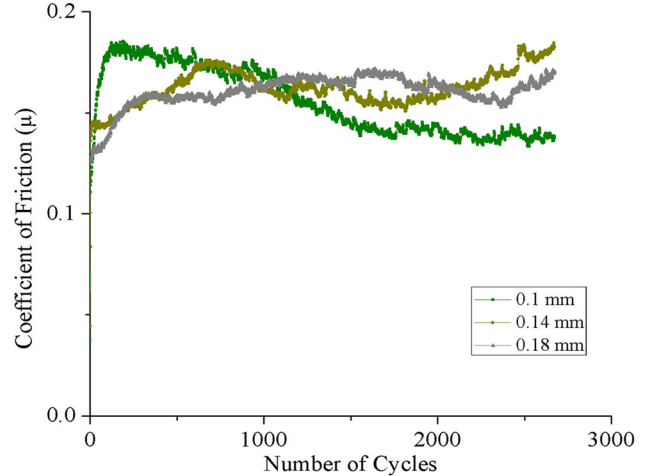


Fig. 17 Variation in COF with number of cycles at 30N and 100 rpm for CFPETG

surface along with some porosity can be seen in Figure 13(c). In Figure 13(d) a clear view of the compression on one side and a tension of the various polymeric layers can be seen prior to the actual fracture.

3.3 Tribological Behavior

3.3.1 Effect of Carbon fiber Reinforcement on COF. Figure 14 and 15 reveal that with the addition of reinforcement as carbon fiber the overall coefficient of friction is reduced which can be accredited to the intrinsic nature of the carbon to act as a self-lubricating material (Ref 67). Moreover,

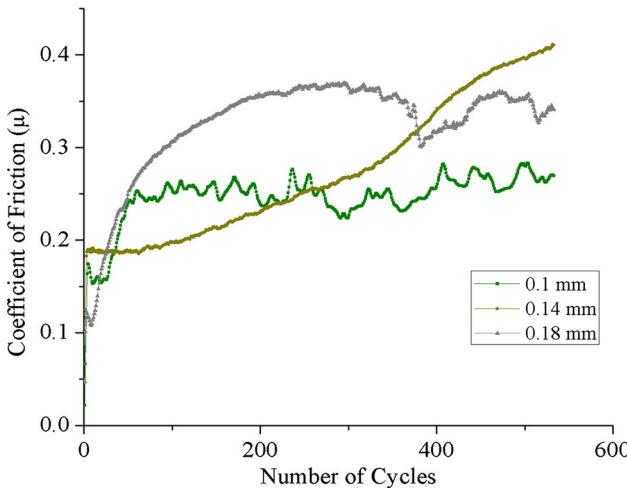


Fig. 18 Variation in COF with number of cycles at 30N and 500 rpm for PETG

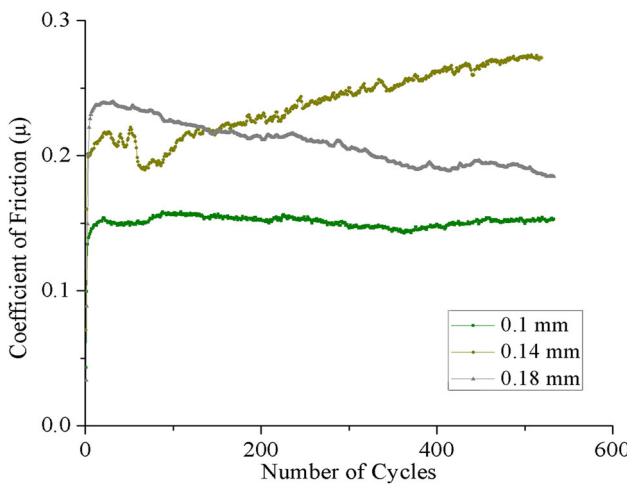


Fig. 19 Variation in COF with number of cycles at 30N and 500 rpm for CFPET

carbon reinforcement adds strength to the polymer matrix, the real contact area with the counter body under load is reduced because of a hard phase in the soft matrix (Ref 68). Due to reduction in true contact area, the layer thickness did not affect the coefficient of friction at different loads for CFPETG. Also, the film formation capability of the carbon fiber (Ref 69) further aided in the reduction the COF even at high speeds.

3.3.2 Effect of Load On COF. As evident from Figure 15 and 16 the COF exhibited an increasing trend with an increase in load. Moreover, the trend is same for both reinforced and non-reinforced PETG polymer, this may be due to increase in area of contact between the polymer sample and steel disk. These results of direct relation of COF with load are in accordance with the studies reported in the literature (Ref 70–72). Increase in load rises the temperature at the interface which results in softening of the polymer material that leads to adhesion and thereby increasing the COF (Ref 73). The tribofilm formed at the interface is also damaged due to higher contact pressures which leads to the increase in COF. The carbon fibers because of having the capability of solid

lubrication, lead to tribofilm formation and hence the friction is lowered in case of lower loads. However, this advantage offered by carbon fiber does not work well at higher loads as the increased pressure leads to breaking of the tribofilm and hence friction increases.

3.3.3 Effect of Speed on COF. From Figure 14 and 15, it can be seen that at low speed the COF is lower than at high speed for both the reinforced and unreinforced PETG. This result may be attributed to the smoothing of the asperities and increase of adhesion at high speeds (Ref 74). Moreover, the effect of rise in temperature with the increasing speed adds to the value of COF. The increased speed also breaks the tribofilm which leads to increase in the COF. These results are in line with Barrett et al. (Ref 75) and Santner et al. (Ref 76).

3.3.4 Effect of Layer Thickness on COF. From Figure 14 and 15, it can be seen that layer thickness 0.18 mm and 0.1 mm exhibited the minimum COF in case of both PETG and CFPETG corresponding to 100 RPM and 500 RPM, respectively. This behavior is the result of the layers touching each other and giving rise to rough boundaries, consequently the high coefficient of friction. Whereas for 0.18 mm layer thickness, the layers fuse into each other as there is no air gap which gives rise to lesser asperities, thereby resulting in the reduced coefficient of friction at lower speed. The results obtained in this case are in line with previous studies (Ref 42). At lower layer thickness, the higher interlayer adhesion between the layers helped to maintain a lower coefficient of friction. As the layer height increases, poor or incomplete adhesion between the layers may result in an increase in the coefficient of friction at high speed (Ref 45).

3.3.5 Variation in Coefficient of Friction With Number of Cycles. The behavior of each layer thickness can be estimated from the graphs of COF against the number of cycles for 30N at 100 and 500 RPM for both PETG and CFPETG. Figure 16 depicts that layer height 0.18 initially increased linearly upto ~1200 cycles after that steady state is attained because of the asperities getting smoothed. The trend followed by 0.1 mm and 0.14 mm layer thickness is almost similar with 0.14mm having maximum COF value because of the more asperities at the interfacial level due to inappropriate bounding. The sharp peaks observed may be due to third body abrasion due to inclusion of wear debris.

Figure 17 depicts that with CFPETG the COF of 0.1 mm layer thickness initially increases followed by a linear decrease upto ~ 1200 cycle and after that a steady state is attained because the asperities gets smoothed after 1200 cycles. Whereas, the other two layer thicknesses 0.14mm and 0.18mm exhibited a different trend and finally 0.14 mm achieving the highest COF value.

Figure 17 reveals a peculiar trend in CFPETG in contrast to PETG, an initial increase in the COF is observed as against a decrease initially in case of PETG. This behavior is due to the property of carbon fiber to lubricate and layer formation capability. The layer formation is indicated after around 200 cycles leading to lowering of COF.

From the curves (Figure 18) obtained for PETG at 30N and 500 rpm, it can be seen that 0.14mm thickness varies linearly with number of cycles because of the adhesion of asperities with the counter body. At layer thickness 0.1mm curve seems to be increasing linearly at the initial cycles because of the excessive ploughing after that due to inclusion of wear debris several peak values are attained upto the end of cycle. The COF curve for 0.18mm layer thickness first increases due to

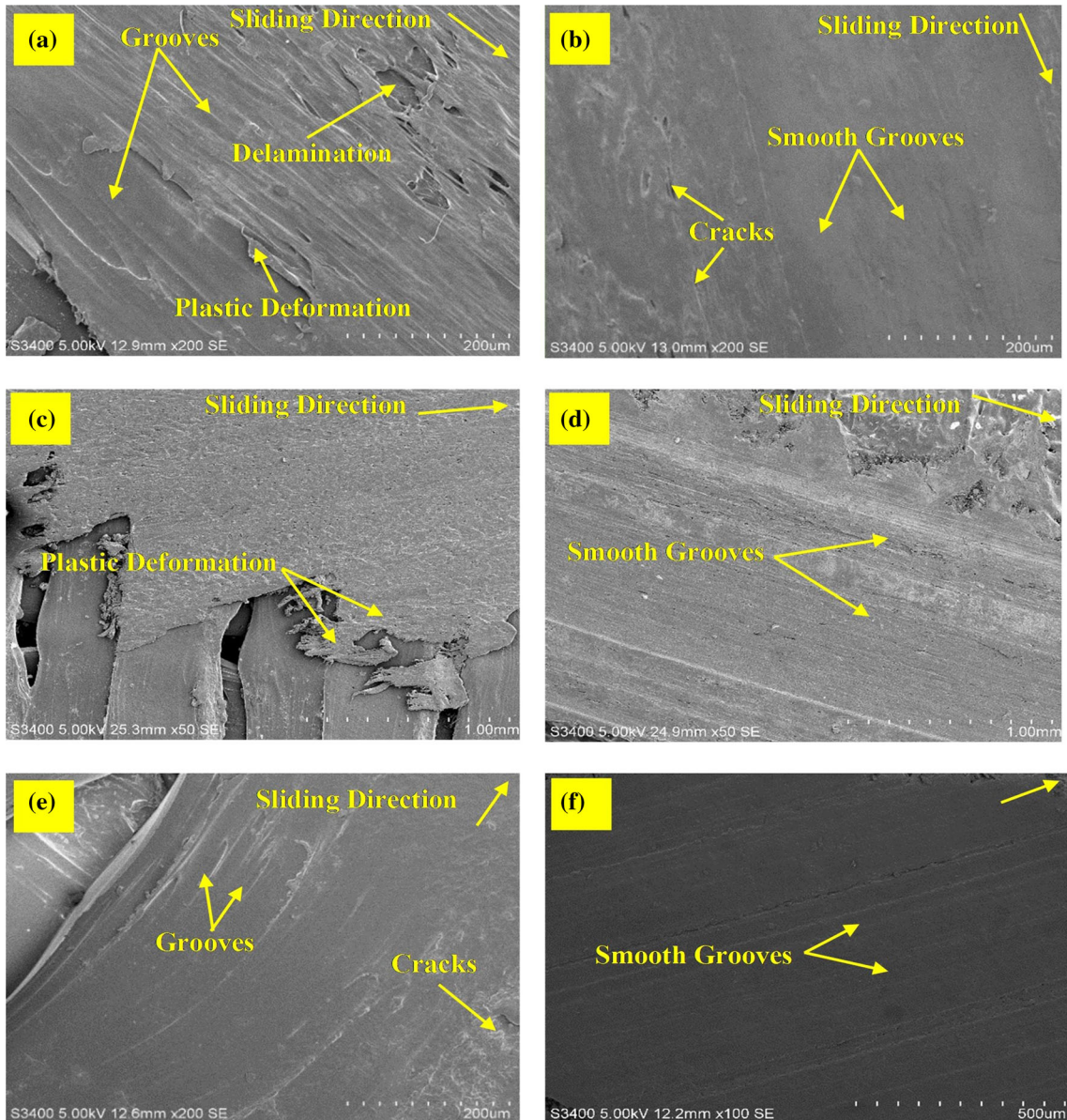


Fig. 20 SEM images of worn out samples (a) grid PETG (b) grid CFPETG (c) triangular PETG (d) triangular CFPETG (e) honeycomb PETG (f) honeycomb CFPETG corresponding to infill percentage of 70% and layer thickness of 0.14mm

adhesion then decreases with a dip at 400 cycles because of the cleared asperities tending toward increasing adhesion. From Figure 19 it can be seen that 0.14mm layer thickness curve increased linearly with the increase in adhesion after some initial variations due to increased asperities and the curve for 0.18mm layer thickness due to gradual smoothening of asperities shows a decreasing trend after initial increase. The steady state is exhibited by 0.1mm layer thickness throughout owing to constant air gaps.

3.3.6 Worn Surface Analysis. Figure 20 shows the SEM images of the worn out surfaces. Distinct wear morphologies for different 3D-printed materials with different reinforcement and infill patterns can be seen from the images. The addition of carbon fibers leads to smoothening of the surfaces as can be seen in Figure 20(b), (d), and (f) in comparison to Figure 20(a), (c), and (e). In case of unreinforced PETG delamination

(Figure 20a), plastic deformation in the direction of sliding (Figure 20c), some deep grooves (Figure 20e) alongwith some cracks on the worn out surface can be observed. Some microcracks and fibers being delaminated can also be seen (Figure 20a and b). The smoothening of the worn out surfaces clearly suggests the role of carbon fibers in lowering friction.

4. Conclusions

1. The addition of carbon fiber as reinforcement 20 wt.% to PETG polymer improved the tensile strength of the printed samples at the layer thickness 0.1mm at all the infill percentages and infill patterns but not at the higher layer thicknesses.

2. CFPETG exhibited maximum 114% increase in tensile strength for triangular pattern with 40% infill percentage and minimum of 43.7% for full honeycomb pattern with 100% infill percentage at layer thickness 0.1mm.
3. The bending strength was also seen to be improved in case of reinforced PETG polymer only at layer thickness 0.18 mm with maximum of 25% at 70% infill percentage for full honeycomb.
4. The COF was reduced because of the CF addition corresponding to all the loads (10, 20, 30, 40, 50N) and speeds (100, 500 RPM). The carbon fiber increased the strength of the polymer and its intrinsic lubricating nature further helped in improving the frictional resistance. The COF was reduced up to 47.3% at 100 RPM at 0.1 mm layer thickness and 44.79% at 500 RPM at 0.18mm layer thickness. Addition of carbon fibers leads to COF reduction due to its film formation capability.
5. The SEM fractographic analysis of the fractured samples in case of tensile and flexural testing revealed distinct fracture modes and morphologies for the tested samples. Further, in case of worn surfaces different wear mechanisms for the developed composites were observed. Further, the role of carbon fibers in smoothening the surfaces is also visible and changing the wear modes from delamination to abrasion.
6. The findings of this work shall help to widen the scope of PETG as an engineering material and shall help the manufacturing community to choose the 3D printing parameters as per the target application.
7. Future research can be undertaken to study the wear behavior of these composites and studying the effect of other parameters on the different mechanical properties.

Authors' Contributions:

AFK involved in methodology and writing original draft. AR participated in supervision, methodology, writing, review, and editing. MIUH involved in conceptualization, supervision, methodology, writing, review, and editing. MSW participated in methodology, writing, review, and editing

Funding

No funding was received for this work.

Conflict of interest

No conflicts of interests between the authors

References

1. M.I.U. Haq, S. Khuroo, A. Raina, S. Khajuria, M. Javaid, M.F.U. Haq et al., 3D Printing for Development of Medical Equipment Amidst Coronavirus (COVID-19) Pandemic—Review and Advancements, *Res. Biomed. Eng.* 2020, p. 1-11
2. A. Chadha, M.I.U. Haq, A. Raina, R.R. Singh, N.B. Penumarti and M.S. Bishnoi, Effect of Fused Deposition Modelling Process Parameters on Mechanical Properties of 3D Printed Parts, *World J. Eng.* 2019
3. Z.U. Baba, W.K. Shafi, M.I.U. Haq and A. Raina, Towards Sustainable Automobiles—Advancements and Challenges, *Prog. Ind. Ecol. an Int. J.*, 2019, **13**, p 315–331.
4. D. I. Yang, C., Cao, Y., Shi, C., Li, A Controlled Cold Deposition 3D Printing Method for PEEK Materials
5. C. Cozmei and F. Caloian, Additive Manufacturing Flickering at the Beginning of Existence, *Procedia Econ. Financ.*, 2012, **3**, p 457–462.
6. C.W.J. Lim, K.Q. Le, Q. Lu and C.H. Wong, An Overview of 3-D Printing in Manufacturing, Aerospace, and Automotive Industries, *IEEE Potentials*, 2016, **35**, p 18–22.
7. L. Zhu, N. Li and P.R.N. Childs, Light-Weighting in Aerospace Component and System Design, *Propuls. Power Res.*, 2018, **7**, p 103–119.
8. T.Q. Duong, E. Korolev and A. Inozemtcev, Selection of Reinforcing Fiber for High-strength Lightweight Concrete for 3D-Printing, in IOP Conference Series: Materials Science and Engineering, 2021 1030, p 12007
9. O.A. Mohamed, S.H. Masood and J.L. Bhowmik, Optimization of Fused Deposition Modeling Process Parameters: A Review of Current Research and Future Prospects, *Adv. Manuf.*, 2015, **3**, p 42–53.
10. S.-H. Ahn, M. Montero, D. Odell, S. Roundy and P.K. Wright, Anisotropic Material Properties of Fused Deposition Modeling ABS, *Rapid Prototyp. J.*, 2002, **8**, p 248–257.
11. J.S. Chohan, R. Singh, K.S. Boparai, R. Penna and F. Fraternali, Dimensional Accuracy Analysis of Coupled Fused Deposition Modeling and Vapour Smoothing Operations for Biomedical Applications, *Compos. Part B Eng.*, 2017, **117**, p 138–149.
12. J. Jordan, K.I. Jacob, R. Tannenbaum, M.A. Sharaf and I. Jasiuk, Experimental Trends in Polymer Nanocomposites—A Review, *Mater. Sci. Eng. A*, 2005, **393**, p 1–11.
13. A.K. Sood, R.K. Ohdar and S.S. Mahapatra, Parametric Appraisal of Mechanical Property of Fused Deposition Modelling Processed Parts, *Mater. Des.*, 2010, **31**, p 287–295.
14. J.N. Coleman, U. Khan and Y.K. Gunko, Mechanical Reinforcement of Polymers Using Carbon Nanotubes, *Adv. Mater.*, 2006, **18**, p 689–706.
15. A. Sharma, S. Kumar, B. Tripathi, M. Singh and Y.K. Vijay, Aligned CNT/Polymer Nanocomposite Membranes for Hydrogen Separation, *Int. J. Hydrogen Energy*, 2009, **34**, p 3977–3982.
16. J. Barrios-Muriel, F. Romero-Sánchez, F.J. Alonso-Sánchez and D. Rodriguez Salgado, Advances in Orthotic and Prosthetic Manufacturing: A Technology Review, *Materials (Basel)*, 2020, **13**, p 295.
17. F. Klocke, A. Klink, D. Veselovac, D.K. Aspinwall, S.L. Soo, M. Schmidt et al., Turbomachinery Component Manufacture by Application of Electrochemical, Electro-Physical and Photonic Processes, *CIRP Ann.*, 2014, **63**, p 703–726.
18. J. Spale, V. Novotny, V. Mares and A.P. Weiß, 3D Printed Radial Impulse Cantilever Micro-Turboexpander for Preliminary Air Testing, in AIP Conference Proceedings, 2021, 2323, p 70002
19. U.R. Tuzkaya et al., A Single Side Priority Based GA Approach for 3D Printing Center Integration to Spare Part Supply Chain in Automotive Industry, *Teh. Vjesn.* 2021, **28**, 836–844
20. C. De Vries, Volkswagen Autoeuropa: Maximizing production efficiency with 3D printed tools, jigs, and fixtures, Ultim. <https://ultimaker.com/en/stories/43969-volkswagen-autoeuropa-maximizing-production-efficiency-with-3d-printed-tools-jigs-and-fixtures> (access 3/3/2019) (2017)
21. A.F. Kichloo, R. Aziz, M.I.U. Haq and A. Raina, Mechanical and Physical Behaviour of 3D printed Polymer Nanocomposites-A Review, *Int. J. Ind. Syst. Eng.*, 2021, **38**, p 484–502.
22. A.D. Mazurchevici, D. Nedelcu, R. Popa et al., Additive Manufacturing of Composite Materials by FDM Technology: A Review, *Indian J. Eng. Mater. Sci.*, 2021, **27**, p 179–192.
23. ASTM, Standard Terminology for Additive manufacturing -General Principles-Terminology. ASTM ISO/ASTM52900-15. West Conshohocken, (2015)
24. R. Aziz, M.I.U. Haq and A. Raina, Effect of Surface Texturing on Friction Behaviour of 3D Printed Polylactic Acid (PLA), *Polym. Test.*, 2020, **85**, p 106434.
25. W.S.W. Harun, S. Sharif, M.H. Idris and K. Kadrigama, Characteristic Studies of Collapsibility of ABS Patterns Produced from FDM for Investment Casting, *Mater. Res. Innov.*, 2009, **13**, p 340–343.
26. N. Naveed, Investigate the Effects of Process Parameters on Material Properties and Microstructural Changes of 3D-Printed Specimens using Fused Deposition Modelling (FDM), *Mater. Technol.* 2020, p 1-14

27. N. Naveed, Investigating the Material Properties and Microstructural Changes of Fused Filament Fabricated PLA and Tough-PLA Parts, *Polymers (Basel.)*, 2021, **13**, p 1487.
28. X. Tian, T. Liu, C. Yang, Q. Wang and D. Li, Interface and Performance of 3D Printed Continuous Carbon Fiber Reinforced PLA Composites, *Compos. Part A Appl. Sci. Manuf.*, 2016, **88**, p 198–205.
29. R. Kumar, M. I. Ul Haq, A. Raina, and A. Anand, Industrial Applications of Natural Fiber Reinforced Polymer Composites - Challenges and Opportunities, *J. Sustain. Eng.* 2018
30. A.C. de Leon, Q. Chen, N.B. Palaganas, J.O. Palaganas, J. Manapat and R.C. Advincula, High Performance Polymer Nanocomposites for Additive Manufacturing Applications, *React. Funct. Polym.*, 2016, **103**, p 141–155.
31. W. Zhong, F. Li, Z. Zhang, L. Song and Z. Li, Short Fiber Reinforced Composites for Fused Deposition Modeling, *Mater. Sci. Eng. A*, 2001, **301**, p 125–130.
32. S. Dul, L. Fambri and A. Pegoretti, Filaments Production and Fused Deposition Modelling of ABS/Carbon Nanotubes Composites, *Nanomaterials*, 2018, **8**, p 49.
33. V.C. Gavali, P.R. Kubade and H.B. Kulkarni, Mechanical and Thermomechanical Properties of Carbon Fibre Reinforced Thermoplastic Composite Fabricated Using Fused Deposition Modelling (FDM) Method: A Review, *Int. J. Mech. Prod. Eng. Res. Dev.*, 2018, **8**, p 1161–1168.
34. R.T.L. Ferreira, I.C. Amatte, T.A. Dutra and D. Bürger, Experimental Characterization and Micrography of 3D Printed PLA and PLA Reinforced with Short Carbon Fibers, *Compos. Part B Eng.*, 2017, **124**, p 88–100.
35. K. Prashantha and F. Roger, Multifunctional Properties of 3D Printed Poly (Lactic Acid)/Graphene Nanocomposites by Fused Deposition Modeling, *J. Macromol. Sci. Part A*, 2017, **54**, p 24–29.
36. B. Coppola, N. Cappetti, L. Di Maio, P. Scarfato and L. Incarnato, Influence of 3D Printing Parameters on the Properties of PLA/Clay Nanocomposites, *AIP Conf. Proc.*, 1981, **2018**, p 20064.
37. Y. Nakagawa, K. Mori and T. Maeno, 3D Printing of Carbon Fibre-Reinforced Plastic Parts, *Int. J. Adv. Manuf. Technol.*, 2017, **91**, p 2811–2817.
38. C. Yang, X. Tian, T. Liu, Y. Cao and D. Li, 3D Printing for Continuous Fiber Reinforced Thermoplastic Composites: Mechanism and Performance, *Rapid Prototyp. J.*, 2017, **23**, p 209–215.
39. I. Ferreira, D. Vale, M. Machado and J. Lino, Additive Manufacturing of Polyethylene Terephthalate Glycol/Carbon Fiber Composites: An Experimental Study from Filament to Printed Parts, *Proc. Inst. Mech. Eng. Part L J. Mater. Des. Appl.* 2018, p. 1464420718795197
40. S. Berretta, R. Davies, Y.T. Shyng, Y. Wang and O. Ghita, Fused Deposition Modelling of High Temperature Polymers: Exploring CNT PEEK Composites, *Polym. Test.*, 2017, **63**, p 251–262.
41. R. Singh, N. Singh, A. Amendola and F. Fraternali, On the Wear Properties of Nylon6-SiC-Al₂O₃ Based Fused Deposition Modelling Feed Stock Filament, *Compos. Part B Eng.*, 2017, **119**, p 125–131.
42. O.A. Mohamed, S.H. Masood and J.L. Bhowmik, A Parametric Investigation of the Friction Performance of PC-ABS Parts Processed by FDM Additive Manufacturing Process, *Polym. Adv. Technol.*, 2017, **28**, p 1911–1918.
43. O.A. Mohamed, S.H. Masood and J.L. Bhowmik, Analysis of Wear Behavior of Additively Manufactured PC-ABS Parts, *Mater. Lett.*, 2018, **230**, p 261–265.
44. K.S. Boparai and R. Singh, Investigations for Enhancing Wear Properties of Rapid Tooling by Reinforcement of Nanoscale Fillers for Grinding Applications, *J. Micro Nano-Manufacturing*, 2018, **6**, p 21004.
45. J. Bustillos, D. Montero, P. Nautiyal, A. Loganathan, B. Boesl and A. Agarwal, Integration of Graphene in Poly (Lactic) Acid by 3D Printing to Develop Creep and Wear-Resistant Hierarchical Nanocomposites, *Polym. Compos.*, 2018, **39**, p 3877–3888.
46. E.G. Ertane, A. Dorner-Reisel, O. Baran, T. Welzel, V. Matner and S. Svoboda, Processing and Wear Behaviour of 3D Printed PLA Reinforced with Biogenic Carbon, *Adv. Tribol.* 2018, 2018
47. K. Wang, X. Xie, J. Wang, A. Zhao, Y. Peng and Y. Rao, Effects of Infill Characteristics and Strain Rate on the Deformation and Failure Properties of Additively Manufactured Polyamide-Based Composite Structures, *Results Phys.*, 2020, **18**, p 103346.
48. M. Kamaal, M. Anas, H. Rastogi, N. Bhardwaj and A. Rahaman, Effect of FDM Process Parameters on Mechanical Properties of 3D-Printed Carbon Fibre-PLA Composite, *Prog. Addit. Manuf.*, 2021, **6**, p 63–69.
49. M. Nachtane, M. Tarfaoui, Y. Ledoux, S. Khammassi, E. Leneveu and J. Pellete, Experimental Investigation on the Dynamic Behavior of 3D Printed CF-PEKK Composite Under Cyclic Uniaxial Compression, *Compos. Struct.*, 2020, **247**, p 112474.
50. K.S. Kumar, R. Soundararajan, G. Shanthosh, P. Saravanakumar and M. Ratteesh, Augmenting Effect of Infill Density and Annealing on Mechanical Properties of PETG and CFPETG Composites Fabricated by FDM, *Mater. Today Proc.*, 2021, **45**, p 2186–2191.
51. K.A.M. Menderes, A. İpekçi and H. Saruhan, Investigation of 3d Printing Filling Structures Effect on Mechanical Properties and Surface Roughness of PET-G Material Products, *Gaziosmanpasa Bilim. Aracstirma Derg.*, 2017, **6**, p 114–121.
52. U.K. uz Zaman, E. Boesch, A. Siadat, M. Rivette and A.A. Baqai, Impact of Fused Deposition Modeling (FDM) Process Parameters on Strength of Built Parts Using Taguchi—s Design of Experiments, *Int. J. Adv. Manuf. Technol.* 2018, p. 1–12
53. M. Fernandez-Vicente, W. Calle, S. Ferrandiz and A. Conejero, Effect of Infill Parameters on Tensile Mechanical Behavior in Desktop 3D Printing, *3D Print Addit. Manuf.*, 2016, **3**, p 183–192.
54. S. Tandon, R. Kacker and K.G. Sudhakar, Experimental Investigation on Tensile Properties of the Polymer and Composite Specimens Printed in a Triangular Pattern, *J. Manuf. Process.*, 2021, **68**, p 706–715.
55. H. Li, T. Wang, J. Sun and Z. Yu, The Effect of Process Parameters in Fused Deposition Modelling on Bonding Degree and Mechanical Properties, *Rapid Prototyp. J.*, 2018, **24**, p 80–92.
56. C. Alvarez, L. Kenny, C. Lagos, F. Rodrigo and M. Aizpun, Investigating the Influence of Infill Percentage on the Mechanical Properties of Fused Deposition Modelled ABS Parts, *Ing. Investig.*, 2016, **36**, p 110–116.
57. S. Hwang, E.I. Reyes, K. Moon, R.C. Rumpf and N.S. Kim, Thermo-Mechanical Characterization of Metal/Polymer Composite Filaments and Printing Parameter Study for Fused Deposition Modeling in the 3D Printing Process, *J. Electron. Mater.*, 2015, **44**, p 771–777.
58. A. Lanzotti, M. Grasso, G. Staiano and M. Martorelli, The Impact of Process Parameters on Mechanical Properties of Parts Fabricated in PLA with an Open-Source 3-D Printer, *Rapid Prototyp. J.*, 2015, **21**, p 604–617.
59. T. Hofstätter, I.W. Gutmann, T. Koch, D.B. Pedersen, G. Tosello, G. Heinz et al., Distribution and Orientation of Carbon Fibers in Polylactic, *Proc. ASPE Summer Top. Meet.* 2016
60. S. Meng, H. He, Y. Jia, P. Yu, B. Huang and J. Chen, Effect of Nanoparticles on the Mechanical Properties of Acrylonitrile-Butadiene-Styrene Specimens Fabricated by Fused Deposition Modeling, *J. Appl. Polym. Sci.* 2017, 134
61. C. Giovedì, L.D.B. Machado, M. Augusto, E.S. Pino and P. Radino, Evaluation of the Mechanical Properties of Carbon Fiber after Electron Beam Irradiation, *Nucl. Inst. Methods Phys. Res. Sect. B Beam Interact. with Mater. Atoms*, 2005, **236**, p 526–530.
62. A.K. Sood, V. Chaturvedi, S. Datta and S.S. Mahapatra, Optimization of Process Parameters in Fused Deposition Modeling Using Weighted Principal Component Analysis, *J. Adv. Manuf. Syst.*, 2011, **10**, p 241–259.
63. X. Yao, C. Luan, D. Zhang, L. Lan and J. Fu, Evaluation of Carbon Fiber-Embedded 3D Printed Structures for Strengthening and Structural-Health Monitoring, *Mater. Des.*, 2017, **114**, p 424–432.
64. O. Luzanin, V. Guduric, I. Ristic and S. Muhic, Investigating Impact of Five Build Parameters on the Maximum Flexural Force in FDM Specimens—a Definitive Screening Design Approach, *Rapid Prototyp. J.*, 2017, **23**, p 1088–1098.
65. N. Li, Y. Li and S. Liu, Rapid Prototyping of Continuous Carbon Fiber Reinforced Polylactic Acid Composites by 3D Printing, *J. Mater. Process. Technol.*, 2016, **238**, p 218–225.
66. G. Wypych, The Effect of Fillers on the Mechanical Properties of Filled Materials, *Handbook of Fillers*, 2016
67. M.I.U. Haq and A. Anand, Dry Sliding Friction and Wear Behaviour of Hybrid AA7075/Si₃N₄/Gr Self Lubricating Composites, *Mater. Res. Express*, 2018
68. Wear principles and resistance of materials. Beijing: Tsinghua University Press, 1993

69. R. Reinicke, F. Haupert and K. Friedrich, On the Tribological Behaviour of Selected, Injection Moulded Thermoplastic Composites, *Compos. Part A Appl. Sci. Manuf.*, 1998, **29**, p 763–771.
70. M.I. Ul Haq and A. Anand, Dry Sliding Friction and Wear Behaviour of Hybrid AA7075/Si₃N₄/Gr Self Lubricating Composites, *Mater. Res. Express*, 2018, **5**, p 066544.
71. M.I. Ul Haq, A. Raina, S. Mohan, A. Anand and M.F. Bin Abdollah, Potential of AA7075 as a Tribological Material for Industrial Applications-A Review, (2021)
72. H.K. Garg and R. Singh, Comparison of Wear Behavior of ABS and Nylon6—Fe Powder Composite Parts Prepared with Fused Deposition Modelling, *J. Cent. South Univ.*, 2015, **22**, p 3705–3711.
73. K.C. Ludema and D. Tabor, The Friction and Visco-Elastic Properties of Polymeric Solids, *Wear*, 1966, **9**, p 329–348.
74. M.I. Ul Haq and A. Anand, Friction and Wear Behavior of AA 7075-Si₃N₄ Composites Under Dry Conditions: Effect of Sliding Speed, Silicon, 2018
75. T.S. Barrett, G.W. Stachowiak and A.W. Batchelor, Effect of Roughness and Sliding Speed on the Wear and Friction of Ultra-High Molecular Weight Polyethylene, *Wear*, 1992, **153**, p 331–350.
76. E. Santner and H. Czichos, Tribology of Polymers, *Tribol. Int.*, 1989, **22**, p 103–109.

Publisher's Note Springer Nature remains neutral with regard to jurisdictional claims in published maps and institutional affiliations.